Reversal in Output Current Direction of 4H-SiC/Cu Tribovoltaic Nanogenerator as Controlled by Relative Humidity

Jinchao Xia, Andy Berbille, Xiongxin Luo, Jiayu Li, Ziming Wang, Laipan Zhu,* and Zhong Lin Wang*

Tribovoltaic nanogenerators (TVNG) represent a fantastic opportunity for developing low-frequency energy harvesting and self-powered sensing, by exploiting their real-time direct-current (DC) output. Here, a thorough study of the effect of relative humidity (RH) on a TVNG consisting of 4H-SiC (n-type) and metallic copper foil (SM-TVNG) is presented. The SM-TVNG shows a remarkable sensitivity to RH and an abnormal RH dependence. When RH increases from ambient humidity up to 80%, an increasing electrical output is observed. However, when RH rises from 80% to 98%, the signal output not only decreases, but its direction reverses as it crosses 90% RH. This behavior differs greatly from that of a Si-based TVNG, whose output constantly increases with RH. The behavior of the SM-TVNG might result from the competition between the built-in electric field induced by metal-semiconductor contact and a strong triboelectric electric field induced by solid-liquid triboelectrification under high RH. The authors also demonstrated that both SM-TVNG and Si-based TVNG can work effectively as-is even fully submerged in deionized water. This mechanism can affect other devices and be applied to design self-powered sensors working under high RH or underwater.

1. Introduction

The rapid development of big data and the Internet of Things is pushing researchers to develop alternatives to traditional sources of energy (electromagnetic power generators, batteries, etc.),[1–3] considering their disadvantages for powering scattered devices across large areas or in some scenarios.[4,5] The characteristics of tribovoltaic nanogenerators (TVNGs)[6] put them at an advantage for harvesting high entropy energy and designing self-powered sensors.[7] Indeed, owing to the tribovoltaic effect, they can deliver a real-time direct current (DC) output, with a high current density and low impedance,[8] by converting mechanical energy into electrical energy similar to the way the photovoltaic effect produces energy from light.[9] The principle of this phenomenon can be described as follows. When a semiconductor material contacts a metal, or another semiconductor with different Fermi levels (E_F), electrons from the material with the highest E_F will spontaneously diffuse to that with the lowest one.[10,11] As a result, a space charge region is formed, and a built-in electric field arises at the interface to balance carriers' diffusion. When a metal and a semiconductor, or two semiconductors, are sliding relatively close to each other, chemical bonds break and reform at the interface.[12] During the formation of interfacial chemical bonds, energy quanta, called bindingtons, are released.[13] Those can excite electron-hole pairs if they possess a sufficient amount of energy. The newly formed charge carriers are then separated by the built-in electric field, which generates a current between the two ends of the device, connected through an external circuit.

Although the research on TVNG is still at an early stage, significant progress has been made both on the fundamental and applicative side.[6,14] However, most of the literature consists of empirical studies that aim at improving the TVNG output by selecting friction materials, [11,15–17] or designing new structures for the devices (dynamic Schottky junctions,[18] p-n junctions,[19,20] liquid-semiconductor,[13] and multi-layer structural junctions[21]). Additionally, some groups studied the influence of environmental factors, such as illumination (photovoltaic

J. Xia, A. Berbille, X. Luo, J. Li, Z. Wang, L. Zhu, Z. L. Wang
CAS Center for Excellence in Nanoscience
Beijing Institute of Nanoenergy and Nanosystems
Chinese Academy of Sciences
Beijing 101400, China
E-mail: zhulaipan@binn.cas.cn; zlwang@gatech.edu
A. Berbille, L. Zhu, Z. L. Wang
School of Nanoscience and Technology
University of Chinese Academy of Sciences
Beijing 100049, China
Z. L. Wang
School of Materials Science and Engineering
Georgia Institute of Technology
Atlanta, GA 30332-0245, USA
Z. L. Wang
Yonsei Frontier Lab
Yonsei University
Seoul 03722, Republic of Korea

effect),[22] temperature (thermoelectric effect),[23] or relative humidity (RH).[24] Among these parameters, the effect of relative humidity varies drastically as a function of the nature of the interfaces used to form the TVNG.[25] However, these papers generally stopped their investigations at the observation and lacked discussions surrounding the mechanism behind the discrepancy in RH dependence that exists between different devices.

In the present work, we have chosen n-type silicon carbide (4H-SiC) as a model for our study of the dependence of the TVNG output on RH. 4H-SiC is a third-generation semiconductor, endowed with high thermal conductivity, high hardness, low dielectric constant, high chemical stability, and other advantages,[26] that lead to its wide adoption in various electronic devices.[27,28] Moreover, in the case of TVNGs, it demonstrated the ability to deliver excellent output performances in harsh environments, which motivated our choice for this study of TVNGs in various RH conditions.[25] Therefore, we built a TVNG based on a Schottky structure fabricated with a nitrogen-doped 4H-SiC single crystal and a metal Cu foil (SM-TVNG) and studied its behavior under varying RH and underwater. We observed an abnormal output dependence on RH from our SM-TVNG. When the ambient RH is raised from 20% to 98%, the output increases at first but then decreases and even reverses beyond 80% RH. In contrast, the electrical output of a similarly designed TVNG based on n-type Si increases almost linearly with rising RH. We also show that SM-TVNG works when it is totally submerged in water. Finally, we described the mechanism behind these findings from two points of view: band structure and electron cloud model. This allows us to unveil the underlying physics behind the intriguing behavior of 4H-SiC-based TVNGs under high RH.

2. Results and Discussion

2.1. Fabrication of the SM-TVNG

The setup allowing for the control of RH during the operation of the TVNG consists of a confined chamber made of acrylic panels, to which we added a vapor channel and two robotic arm channels (see **Figure 1**a). The structure of the SM-TVNG is shown in Figure 1b-i. The semiconductor part of the TVNG consists of a 1×1 cm^2 4H-SiC slider (Figure 1b-ii), with a silver (Ag) back electrode that overlaps on the edges of 4H-SiC (Figure 1b-iii), and the ensemble supported by a piece of acrylic. To form the TVNG, the semiconducting part is brought into contact with a copper (Cu) electrode (8×10 cm^2) placed on a piece of acrylic (Figure 1b-iv). In Figure 1c,d, we reported the voltage and current signals recorded when a vertical force of 2 N is applied perpendicularly to the SM-TVNG, while sliding at a speed of 0.1 ms^{-1}, with a delay of 1 s between each stroke. Before conducting the experiment, the oxide layer at the surface of 4H-SiC and Cu are chemically etched. At room temperature, normal air pressure (1 atm) and ambient RH (48%), the open-circuit voltage (V_{oc}) and short-circuit current (I_{sc}) reach 2.85 V and 3.10 µA, respectively (see Figure 1c,d). For RH beyond 85%, we observe a decrease in the signal output by the SM-TVNG, as shown in Figures 1e,f. Interestingly, when the RH of the confined chamber further increases from 85% to 90%, the V_{oc} and I_{sc} signals continue to decrease gradually, but then reverse to an opposite direction and increase slightly along the now reversed direction.
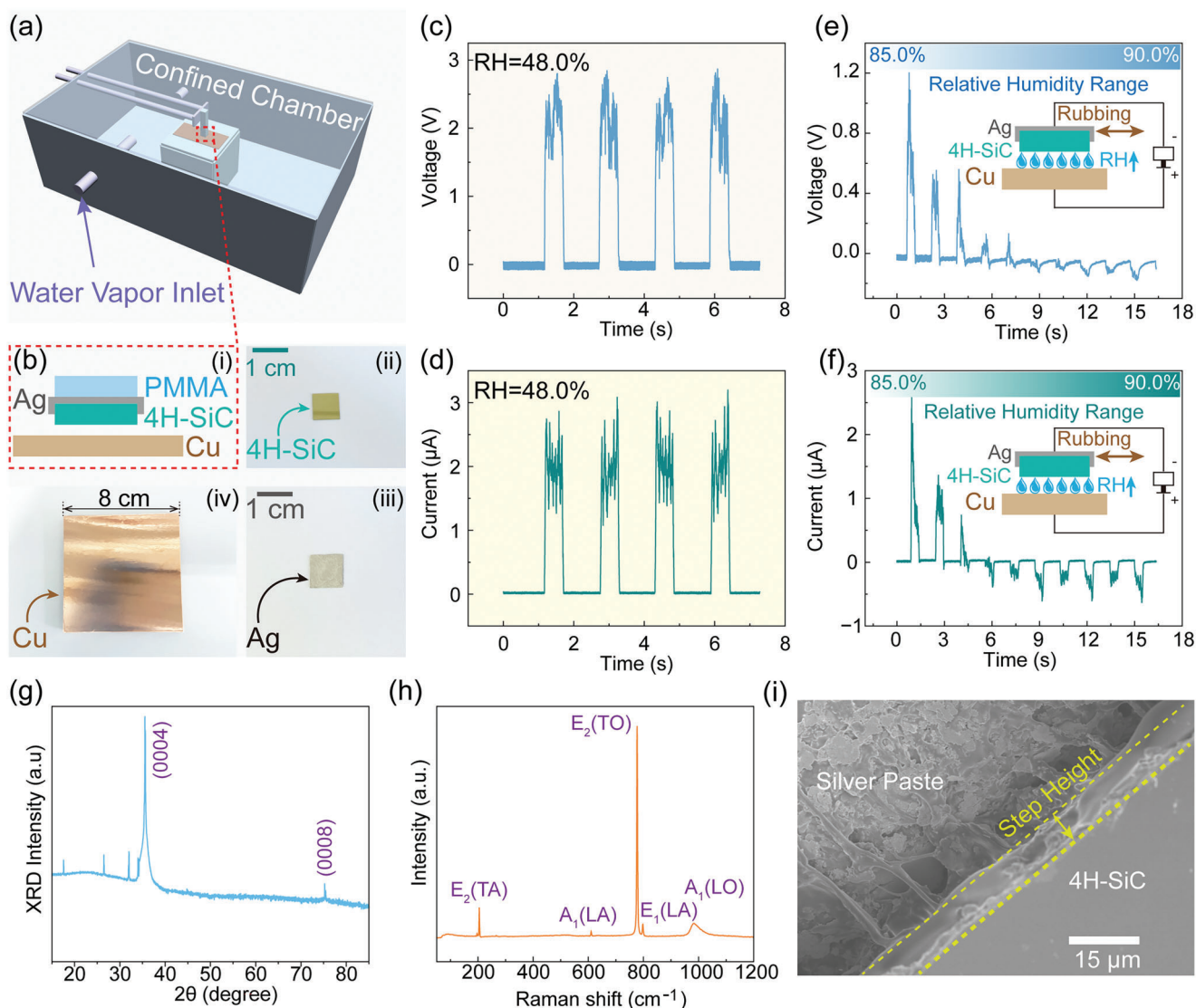
The 4H-SiC slider was characterized before and after the experiment. The X-ray diffraction (XRD) pattern and Raman spectrum, presented in Figure 1g,h, confirmed 4H-SiC's crystal structure.[29,30] In addition, cross-sectional photography of the 4H-SiC was obtained by scanning electron microscopy (SEM) (Figure 1i), to confirm the silver paste is evenly applied and conforms to the side of 4H-SiC. An obvious step between the silver paste and 4H-SiC in the direction perpendicular to the 4H-SiC plane can be observed, which has been deliberately designed to prevent short circuits in the device. It is essential to ensure the overlapping electrode closely fits the side of the 4H-SiC to obtain the best output from the device, An example of a badly fitting electrode is reported in Figure S1a, Supporting Information. Scratches on the surface of Cu foil and 4H-SiC appear at the surface of both materials after the experiment, as shown in Figures S1b,S1c, Supporting Information. It is worth noting the scratches observed at the surfaces of 4H-SiC are deeper and thinner than at the surface of Cu, owing to the greater hardness of 4H-SiC. The sides and surface changes of 4H-SiC before and after coating silver paste electrodes were examined by SEM, as shown in Figure S2, Supporting Information. These images show the case of a properly applied conductive silver paste electrode, covering only the back of the semiconductor and a part of the sides.

2.2. Abnormal RH Dependence of SM-TVNG

The RH dependence of the SM-TVNG's output was studied by precisely controlling RH in a confined chamber. The whole environment is stabilized at various RHs, prior to the measurement of the SM-TVNG's output. As shown in **Figure 2**a, the current is recorded for an SM-TVNG subjected to a vertical force of 2 N, with a horizontal sliding speed of the top layer of 0.1 m/s. In those conditions, when the ambient RH is maintained at 20.0%, 56.5%, 61.5%, 66.5%, 71.5%, 76.5%, 81.5%, and 86.5%, the corresponding I_{sc} reaches ≈0.28, 1.21, 1.43, 1.63, 2.09, 2.30, 3.05, and 2.24 µA. If the ambient RH increases further, we observe a transition of the signal from forward to reverse directions. A relationship between RH and peak current was then extracted, as shown in Figure 2b. The current output corresponding to different RH was linearly fitted to obtain the humidity sensitivities of the 4H-SiC-based TVNG, S_H. The trend in S_H change can be divided into two stages, $S_{H1} = 0.040$ µA/% and $S_{H2} = -0.214$ µA/%.

We also measured the $I–V$ curve characteristics of the device under various RH (Figure 2c). With the increase of RH, the $I–V$ rectifying characteristics of SM-TVNGs improve and their internal resistance decreases. This phenomenon could derive from the presence of water vapor at the interface of the device. Indeed, the increase in RH enhances the surface states of 4H-SiC, owing to the diffusion of water molecules in the slightly porous structures of 4H-SiC. As a result, the Schottky barrier height is enhanced.[31,32] Moreover, when the RH is continuously increased during the operation of the SM-TVNG, we still observe the enhancement of the Schottky rectifying behavior in the device, as shown in Figure S3, Supporting Information.

In addition, by continuously increasing the RH, we identified the tipping point from which the direction of the signals of the SM-TVNG transition from forward to reverse. As shown in Figure 2d, when the RH gradually increases. From 82.6% and

**ADVANCED
SCIENCE NEWS**
www.advancedsciencenews.com

NANO · MICRO
small
www.small-journal.com

Figure 1. Structure, electrical performance test, and material characterization of the 4H-SiC TVNGs. a) Schematic diagram of the humidity tunable chamber and test principle. b) Schematic of the 4H-SiC TVNG structure, and optical images of the 4H-SiC chip (1×1 cm^2), metal copper foil (8×8 cm^2), and silver-coated 4H-SiC chip. c,d) Open-circuit voltage and short-circuit current of the SM-TVNG at room humidity (48%). e,f) Output changes of the open-circuit voltage and short-circuit current of SM-TVNG under continuously increasing humidity. g) Powder XRD pattern and h) Raman spectrum of the 4H-SiC material. i) SEM image of silver electrode distribution on the side of 4H-SiC sheet.

upward, the output always decreases. This sudden change in the behavior of the device could be explained by the change in wettability of 4H-SiC's surface in high RH. As shown in Figure S4, Supporting Information, we observe a sharp decrease of the contact angle at 4H-SiC's surface when RH increases from 80% to 90%. At around 90.0%, another critical point is reached, at which the forward and reverse outputs are equal, resulting in a null output. Beyond 90%, a reversed output signal appears and further increases slightly along the reversed direction and finally plateaued. A detailed representation of the output at around 90% is reported in Figure 2d-i, while the change of RH in the whole process is shown in Figure 2d-ii. We also demonstrated the SM-TVNG still functions when it is submerged in deionized water without any

packaging treatment. Detailed V_{oc} and I_{sc} characteristics of the device underwater are reported in Figure 2e,f, respectively. The SM-TVNG outputs a stable voltage of 0.07 V and a current of 2.32 µA in deionized water. The increased current output compared with that in air is probably due to an increased charge transfer, and reduced internal resistance, in the presence of interfacial water. The data reported in Figure S5, Supporting Information show the stability of the output of the SM-TVNG in deionized water. However, it is important to mention that, when submerged in brine (NaCl, 35 g L^{-1}), the device does not output any current or voltage (Figure S6, Supporting Information). Indeed, the high conductivity of brine, compared to deionized water, causes a short circuit.
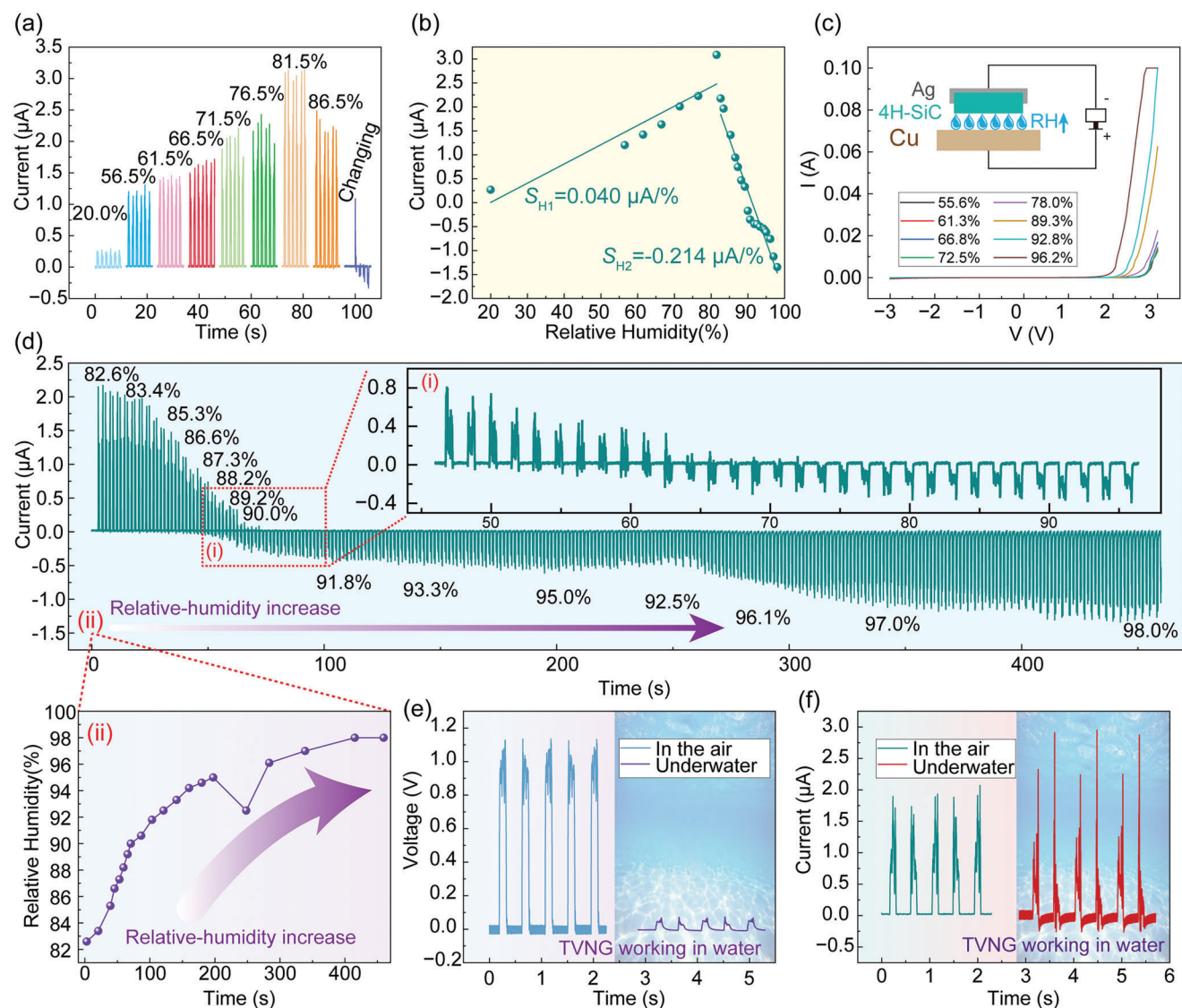
Figure 2. The change of output, sensitivity, and I-V characteristics of SM-TVNG under different RH. a) Short-circuit current when the RH ranges from 20.0% to 86.5%. b) Humidity sensitivity obtained from the relationship between open-circuit current and relative humidity. c) *I–V* characteristics of the SM-TVNG under different humidity conditions. d) Short-circuit current signal with RH ranging from 82.6% to 98.0%. Comparison of output e) voltage and f) current of the SM-TVNG in the air and underwater.
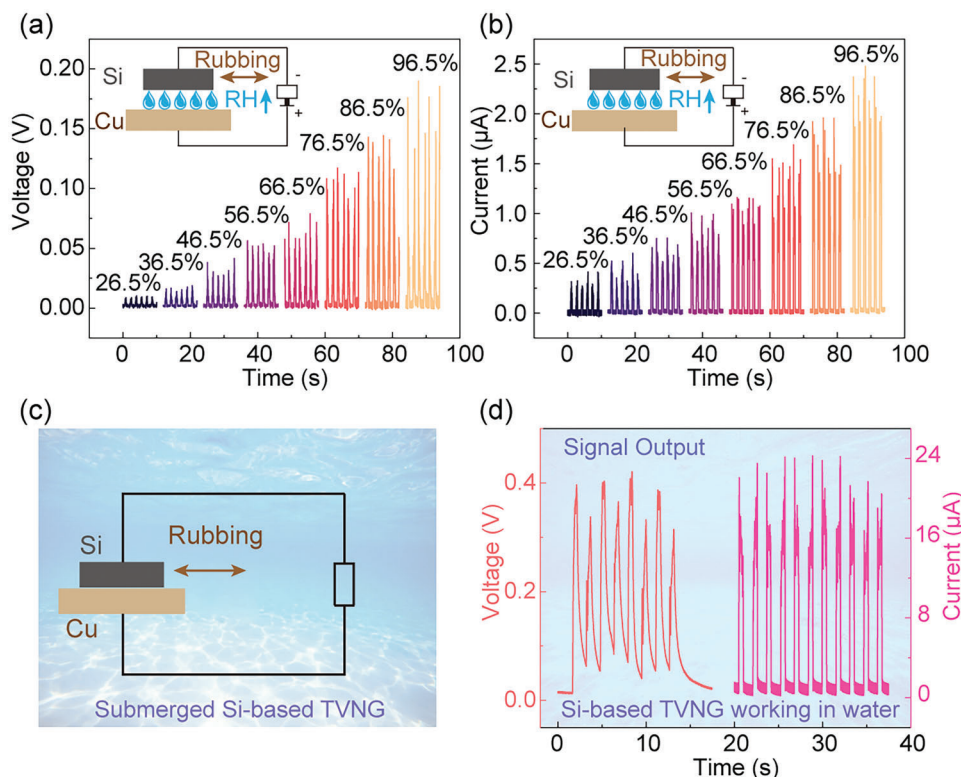
2.3. Comparison of SM-TVNG and Si-Based TVNG

For comparison, we reproduced similar experiments with n-type silicon (n-type Si) as a slider, using an identical structure. **Figure 3**a,b shows the dependence of the output of the Si-based TVNG (Cu as the bottom layer and Si as the top layer) on RH. The sliding velocity of the slider (Si) is 0.1 m s^{-1}, the acceleration is 2 m s^{-1}, the force is 2 N in the vertical direction, and the sliding distance is 50 mm. The V_{oc} and I_{sc} of the Si-based TVNG increase continuously with increasing RH, on the whole measured range of RH. This observation is quite different from that of the SM-TVNGs, indicating the mechanisms of these two devices may differ fundamentally. Furthermore, without any packaging, the Si-based TVNG was submerged and operated in similar conditions to the previous underwater experiment. As shown in Figure 3c,

we also observe that the Si-based TVNG can also work normally in deionized water with an output in the same order of magnitude as that in air, as shown in Figure 3d.

2.4. Working Principle of SM-TVNG

Illustrations of the proposed mechanism behind the abnormal response to humidity of the SM-TVNGs are shown in **Figure 4**. Based on the tribovoltaic effect, when a 4H-SiC chip and Cu foil are in close contact, electrons spontaneously diffuse at the interface, forming a space charge region and an interfacial built-in electric field (E_{in}). Owing to the work function difference between Cu and 4H-SiC ($W_m > W_s$), and the presence of large surface states at the surface of 4H-SiC, the direction of

**ADVANCED
SCIENCE NEWS**

www.advancedsciencenews.com

**NANO · MICRO
small**

www.small-journal.com

Figure 3. Variation of the output of the Si-based TVNG with RH. a,b) Output of open-circuit voltage and short-circuit current of the Si-based TVNG as a function of RH. c) Working diagram of the submerged Si-based TVNG. d) Underwater output of the Si-based TVNG.

built-in electric field at the Schottky junction points from 4H-SiC to Cu, with an upward bending interfacial barrier in 4H-SiC. When 4H-SiC slides on the surface of Cu, new chemical bonds (short-lived) form and break at the interface.[10,13] The formation of short-live chemical bonds at the interface releases energy quanta called "bindington".[13] As shown in Figure 4a, when the bindingtons possess sufficient energy they excite electrons from the valence band to the conduction band, forming electron-hole pairs in the space charge region. The built-in electric field separates the electron-hole pairs in opposite directions, which generates a continuous DC current. When RH increases, the surface state density of 4H-SiC increases, which raises the Schottky barrier height (Figure 4b). The higher Schottky barrier enhances the built-in electric field, thus increasing the driving force for the transport of charge carriers, and the voltage and current. Concurrently, an increased RH also reduces the internal resistance of the SM-TVNG, which leads to an increased output signal. However, if RH continues to increase beyond 80%, then the value of the output starts to decrease. And, with a further increase, the output current reverses and increases in this new direction, until saturation is reached. This remarkable behavior could be explained by the influence of triboelectrification at water-solid interfaces, in the presence of interfacial water in high RH conditions.

We propose that, in a high RH environment, water accumulates in the gaps at the interface of 4H-SiC and Cu, as shown in Figure 4c-i. This water in the gaps can negatively charge the surface of 4H-SiC by contact-electrification (Figure S7, Supporting Information).[12,33] The tribocharges thus generated on the 4H-
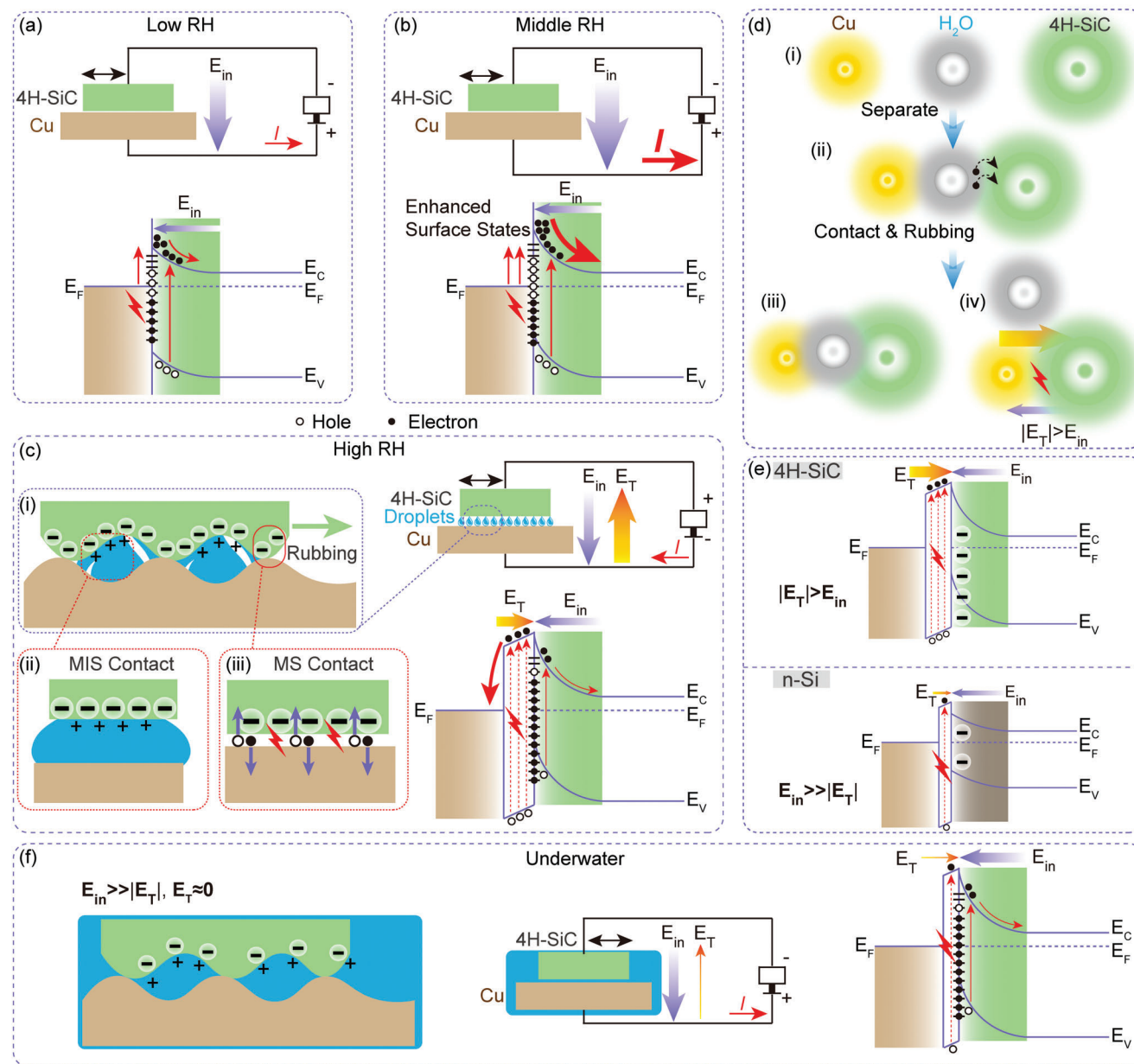
SiC surface create an electric field at the 4H-SiC/Cu interface, which we call E_{SC} (Figure 4c-ii). It should be mentioned that the water is then slightly positively charged. The gradient of charges of charges from one solid surface to another in water generates an electric field named E_W, that opposes E_{SC}. The electric field resulting from the interaction of E_{SC} and E_W, between Cu and the charged surface of 4H-SiC is called "triboelectric electric field" (E_T). E_T points from Cu to 4H-SiC, opposing the built-in electric field (E_{in}) generated by the tribovoltaic effect. The relations between those electric fields are described as follows.

$$E_T = E_{SC} + E_W \tag{1}$$

$$E_{SC} = -nE_W \tag{2}$$

where n belongs to the set of positive real numbers. The charges accumulated at the surface by water-solid triboelectrification are constantly renewed during the friction process, as long as the high RH is maintained. Under high RH, the strength of E_T surpasses that of E_{in} ($|E_T| > E_{in}$). Consequently, in high RH, E_T acts as the driving force that separates electron-hole pairs when a precharged 4H-SiC protuberating morphological defect contacts Cu, as shown in Figure 4c-iii. Thus, the device outputs a DC current in the external circuit with an opposite direction to that obtained in low RH and mild RH (mid-RH) conditions (where the E_{in} dominated).

It is worth noting a part of the triboelectric electric field is canceled by the electrical double layers that form in the water

**ADVANCED
SCIENCE NEWS**

www.advancedsciencenews.com

**NANO · MICRO
small**

www.small-journal.com

Figure 4. Diagrams representing the working principle of the SM-TVNG under different RH, under deionized water, and the physical pictures of the positive/reverse signals. a,b) Energy band analysis of the SM-TVNG under low and middle RH conditions. c) Principle of the positive/reverse output under high RH conditions. d) Diagram of electron cloud model of the SM-TVNG at different RH. e) Comparison of electric fields between the SM-TVNG and the Si-TVNG under high RH. f) Principle of the output under deionized water.

near the charged surfaces of the silicon carbide. This could explain why the negative signal obtained in high RH does not reach the same absolute values as the positive signal obtained in low-RH and mid-RH conditions (Figure 2d). In other words, as illustrated in Figure 4c-ii,iii, we propose that a metal-semiconductor (MS) contact turns to a metal-water-semiconductor (MIS) contact when the RH increases from middle to high when 4H-SiC is used in the TVNG. In this case, we would observe a decreased strength of E_{in} while the strength of E_T increases, that is, $|E_T| > E_{in}$.

The mechanisms of pre-charging and electric field canceling can also be described from the perspective of the overlap of elec-

tron clouds, as shown in Figure 4d. Before contacting, the electron clouds of Cu, water, and 4H-SiC do not overlap (Figure 4d-i). When Cu and 4H-SiC are brought into a high RH environment the electron clouds of the Cu and the 4H-SiC do not overlap with each other. However, they overlap with the electron clouds of water molecules constituting the interfacial water layer (Figure 4d-ii). During the overlap of electron clouds, electrons can be transferred from water to 4H-SiC. In high RH, when water accumulates in the gap between 4H-SiC and Cu (the 4H-SiC and Cu are not in direct contact), a part of E_{SC} is shielded by the electric field (E_W) generated by the gradient of charges in water. Simply put,

the change in RH causes the change in the value of E_T (Figure 4d-iii). We define the total electric field (E_{total}) as the sum of the electric field (E_T) across the interface generated by tribocharges and the built-in electric field (E_{in}).

$$E_{total} = E_T + E_{in} \tag{3}$$

We can then describe the whole process of the variations of the interfacial electric field, according to RH, as follows. First, E_{in} gradually increases as RH rises from about 20% to 80%, owing to increased surface states on 4H-SiC. As a result, E_{total} gradually increases ($E_{in} \gg |E_T|$), which leads to an increased output signal from the SM-TVNG. However, from around 80% to 90%, E_T increases owing to the increased E_{SC} caused by water/SiC contact electrification, from mid-RH to high RH ($E_W \approx 0$). As a result, E_{total} decreases ($E_{in} > |E_T|$), resulting in a gradually decaying output of SM-TVNG. When RH reaches around 90%, E_T is equal to E_{in} ($|E_T| = E_{in}$), leading to a null E_{total}. When $E_{total} = 0$, the SM-TVNG does not deliver any output signal. But as RH goes beyond 90%, E_T overcomes E_{in}. This results in an increase of E_{SC} caused by the tribocharging of 4H-SiC's surface in high RH ($|E_T| > E_{in}$) after separation from the interfacial water (Figure 4d-iv). At this stage, the sign of the output of the SM-TVNG is reversed ($E_{total} < 0$, and $E_{SC} \gg E_W$).

As mentioned previously, Si-based TVNG can also work in a high RH environment. The working mechanism (energy band analysis) is shown in Figure S8, Supporting Information. However, the output of Si-based TVNG always increases with increasing RH. Indeed, in contrast to the case of 4H-SiC, the surface states and barrier for n-Si are relatively lower.[34,35] Thus, negative surface charges can easily migrate to the bulk of n-Si, be ejected, or leaked, which leads to a negligible E_T compared to E_{in} (i.e., $E_{in} \gg E_T$). In this case, the opposite current is not observed, as shown in Figure 4e. Finally, if the SM-TVNG is submerged in deionized water (Figure 4f), the water will facilitate the transfer of charges at the interface between the metal and semiconductor, and part of the triboelectric field will be canceled by the formation of the electrical double layer near 4H-SiC. In this case, $|E_T| \ll E_{in}$, which leads to an electrical current in the same direction as E_{in}.

3. Conclusion

We fabricated an SM-TVNG, composed of 4H-SiC and Cu foil, a device whose output characteristics are greatly influenced by the change of RH. For the SM-TVNG, RH sensitivities reach 0.040 µA/% for RH below 80% and −0.214 µA/% for RH above 80%, respectively. V_{oc} and I_{sc} first increase and then decrease with the increasing humidity from low RH (20.0%) to high RH (90.0%). And, as the RH continues to increase (≥90.0%), the signal eventually reverses and further increases in the opposite direction. The output signal saturates at the maximum RH of 98.0%. The effect of RH on the 4H-SiC/Cu TVNG was explained by a coupling of the built-in electric field created by the tribovoltaic effect and a triboelectric electric field induced by solid-liquid triboelectrification under high RH. Meanwhile, the SM-TVNG placed directly in deionized water, in the absence of packaging, could still output electrical signals in the same order of magnitude as that in air. However, the output of a Si-based TVNG

always increases with increasing humidity, without experiencing a reversal in the direction of current in very high RH. We propose the reason for the different behaviors between the SM-TVNG and the Si-TVNG results from discrepancies in the coupling of the built-in electric field and the triboelectric electric field between those devices. In this work, we focused on studying and describing the physical picture of the phenomena dictating the behavior of the 4H-SiC-based TVNGs in high RH. We suspect this new physical effect could affect other TVNG devices, which represent a significant opportunity for the development of TVNGs as self-powered sensors under high RH, or underwater with potential applications in environmental monitoring and risk control.

4. Experimental Section

Samples, Characterization, and Measurements: Parameters of the as-used 4H-SiC wafer purchased from Jiangyin Haorui Optoelectronics New Materials Co., Ltd. were as follows: crystal orientation (off-axis 4.0° toward <1120> ± 0.5˚), diameter (50.8 ± 0.5 mm), thickness (350 ± 25 µm), and resistivity (< 0.1 Ω cm with nitrogen-doped). Parameters of the n-Si wafer purchased from Suzhou Jinggui Technology Co., Ltd. were as follows: diameter (100 ± 0.3 mm), thickness (525 ± 25 µm), type/orientation (n-type/<100>), and resistivity (20–50 Ω cm). The RH was controlled by a humidifier (LRRGE HUMIDIFIER Air Plus+X12). The process of periodic work of SM-TVNG was maintained by a linear motor (LINMOT 1100). The signals of voltage, current, and charge were obtained by an electrometer and high-resistance meter (Keithley 6514 and 6517B). The RH was measured by a hygrothermograph (GSP-8A). The vertical force was measured by a force sensor (SBT951-T). SEM images were taken by cold-field scanning electron microscopy (HITACHI, SU8020). XRD and Raman data were measured by an X-ray diffractometer (PANalytical B.V., Xpert3 Powder) and a Raman spectrometer (HORIBA JY, LabRAM HR Evolution). A thin layer of gold (Au) was deposited onto the surface of the n-Si by magnetron sputtering equipment (Denton, Discovery635) as a back electrode. The I–V curve was acquired from a semiconductor characterization system (Keithley 4200-SCS). The surface scratches were photographed with an optical microscope (ZEISS Axio Imager M2m).

Statistical Analysis: Basic parameters of 4H-SiC and Si wafers were obtained from the suppliers who offered the wafers. All structural characterization data and electrical performance data were exhibited without the use of transformation, standardization, evaluation of outliers, or other pre-processing methods. The average current values under each RH in Figure 2b were abstracted from six separate sampling periods (*n* = 6) as shown in Figure 2a.

Supporting Information

Supporting Information is available from the Wiley Online Library or from the author.

Conflict of Interest

The authors declare no conflict of interest.

Data Availability Statement

The data that support the findings of this study are available from the corresponding author upon reasonable request.

Keywords

[1] Z. Zhang, H. Wang, T. J. Jacobsson, J. Luo, *Nat. Commun.* **2022**, *13*, 7639.
[2] L. Portilla, K. Loganathan, H. Faber, A. Eid, J. G. D. Hester, M. M. Tentzeris, E. Cantatore, C. Jiang, A. Nathan, G. Fiori, T. Ibn-Mohammed, T. D. Anthopoulos, V. Pecunia, *Nat. Electron.* **2023**, *6*, 10.
[3] S. Westlake, C. H. D. John, E. Cox, *Nat. Energy* **2023**, *8*, 149.
[4] S. Sudevalayam, P. Kulkarni, *IEEE Commun. Surv. Tutorials* **2011**, *13*, 443.
[5] M.-H. Zhang, H. Ding, S. Egert, C. Zhao, L. Villa, L. Fulanović, P. B. Groszewicz, G. Buntkowsky, H.-J. Kleebe, K. Albe, A. Klein, J. Koruza, *Nat. Commun.* **2023**, *14*, 1525.
[6] J. Liu, A. Goswami, K. Jiang, F. Khan, S. Kim, R. McGee, Z. Li, Z. Hu, J. Lee, T. Thundat, *Nat. Nanotechnol.* **2018**, *13*, 112.
[7] S. Lin, Z. L. Wang, *Mater. Today* **2022**, *62*, 111.
[8] J. Meng, C. Pan, L. Li, Z. H. Guo, F. Xu, L. Jia, Z. L. Wang, X. Pu, *Energy Environ. Sci.* **2022**, *15*, 5159.
[9] M.-M. Yang, D. J. Kim, M. Alexe, *Science* **2018**, *360*, 904.
[10] M. Zheng, S. Lin, L. Xu, L. Zhu, Z. L. Wang, *Adv. Mater.* **2020**, *32*, 2000928.
[11] Z. Zhang, D. Jiang, J. Zhao, G. Liu, T. Bu, C. Zhang, Z. L. Wang, *Adv. Energy Mater.* **2020**, *10*, 1903713.
[12] Z. L. Wang, A. C. Wang, *Mater. Today* **2019**, *30*, 34.
[13] S. Lin, X. Chen, Z. L. Wang, *Chem. Rev.* **2021**, *122*, 5209.
[14] C. Xu, J. Yu, Z. Huo, Y. Wang, Q. Sun, Z. L. Wang, *Energy Environ. Sci.* **2023**, *16*, 983.
[15] X. Luo, L. Liu, Y. C. Wang, J. Li, A. Berbille, L. Zhu, Z. L. Wang, *Adv. Funct. Mater.* **2022**, *32*, 2113149.
[16] H. Yuan, Z. Xiao, J. Wan, Y. Xiang, G. Dai, H. Li, J. Yang, *Adv. Energy Mater.* **2022**, *12*, 2200550.
[17] Z. Wang, Z. Zhang, Y. Chen, L. Gong, S. Dong, H. Zhou, Y. Lin, Y. Lv, G. Liu, C. Zhang, *Energy Environ. Sci.* **2022**, *15*, 2366.
[18] X. Huang, X. Xiang, J. Nie, D. Peng, F. Yang, Z. Wu, H. Jiang, Z. Xu, Q. Zheng, *Nat. Commun.* **2021**, *12*, 2268.
[19] R. Xu, Q. Zhang, J. Y. Wang, D. Liu, J. Wang, Z. L. Wang, *Nano Energy* **2019**, *66*, 104185.
[20] Z. Zhang, Z. Wang, Y. Chen, Y. Feng, S. Dong, H. Zhou, Z. L. Wang, C. Zhang, *Adv. Mater.* **2022**, *34*, 2200146.
[21] L. Zhang, H. Cai, L. Xu, L. Ji, D. Wang, Y. Zheng, Y. Feng, X. Sui, Y. Guo, W. Guo, *Matter* **2022**, *5*, 1532.
[22] M. Zheng, S. Lin, Z. Tang, Y. Feng, Z. L. Wang, *Nano Energy* **2021**, *83*, 105810.
[23] Z. Zhang, T. He, J. Zhao, G. Liu, Z. Wang, C. Zhang, *Mater. Today Phys.* **2021**, *16*, 100295.
[24] Z. Wang, L. Gong, S. Dong, B. Fan, Y. Feng, Z. Zhang, C. Zhang, *J. Mater. Chem. A* **2022**, *10*, 25230.
[25] J. Xia, X. Luo, J. Li, L. Zhu, Z. L. Wang, *ACS Appl. Mater. Interfaces* **2022**, *14*, 55192.
[26] M. E. Levinshtein, S. L. Rumyantsev, M. S. Shur, *Properties of Advanced Semiconductor Materials: GaN, AlN, InN, BN, SiC, SiGe*, Wiley, Hoboken, NJ **2001**.
[27] J.-F. Wang, L. Liu, X.-D. Liu, Q. Li, J.-M. Cui, D.-F. Zhou, J.-Y. Zhou, Y. Wei, H.-A. Xu, W. Xu, W.-X. Lin, J.-W. Yan, Z.-X. He, Z.-H. Liu, Z.-H. Hao, H.-O. Li, W. Liu, J.-S. Xu, E. Gregoryanz, C.-F. Li, G.-C. Guo, *Nat. Mater.* **2023**, *22*, 489.
[28] K. C. Miao, A. Bourassa, C. P. Anderson, S. J. Whiteley, A. L. Crook, S. L. Bayliss, G. Wolfowicz, G. Thiering, P. Udvarhelyi, V. Ivády, H. Abe, T. Ohshima, Á. Gali, D. D. Awschalom, *Sci. Adv.* **2019**, *5*, aay0527.
[29] Y. Yin-Tang, H. Ru, *Chin. Phys. B* **2008**, *17*, 3459.
[30] M. Kanaya, J. Takahashi, Y. Fujiwara, A. Moritani, *Appl. Phys. Lett.* **1991**, *58*, 56.
[31] P. Fastykovsky, A. Mogilnitsky, *Sens. Actuators, B* **1999**, *57*, 51.
[32] S. Kozlov, V. Kiselev, Y. F. Novototskii-Vlasov, *Surf. Sci.* **1971**, *28*, 395.
[33] Z. Tang, S. Lin, Z. L. Wang, *Adv. Mater.* **2021**, *33*, 2102886.
[34] J. C. Hill, A. T. Landers, J. A. Switzer, *Nat. Mater.* **2015**, *14*, 1150.
[35] S. Rajput, M. X. Chen, Y. Liu, Y. Y. Li, M. Weinert, L. Li, *Nat. Commun.* **2013**, *4*, 2752.

2305303 (8 of 8)